Osman, A. S., Bolton, M. D. & Mair, R. J. (2006). *Géotechnique* **56**, No. 9, 597–604

Predicting 2D ground movements around tunnels in undrained clay

A. S. OSMAN*, M. D. BOLTON† and R. J. MAIR†

A new analytical method is introduced for calculating displacements due to tunnelling. This is conceived within the framework of the bound theorems of plasticity, but allowing for soil strain-hardening. The ground displacements due to tunnelling are idealised by a simple displacement mechanism of distributed shearing in the plane of the tunnel cross-section. The tunnel support pressure corresponding to a certain volume loss is calculated from energy balances of the work dissipated in distributed shear, the potential energy loss of soil flowing into the tunnel, and the work done by this soil against the tunnel support pressure. The calculations are carried out in steps of small volume loss accompanying small reduction in support pressure, after each of which the tunnel geometry is updated. In this way, each reduced tunnel support pressure is related to a complete ground displacement field. A simplified closed-form solution is also provided for the prediction of maximum surface ground settlement for the particular case of deep tunnelling. This closed-form solution is obtained by integrating the vertical equilibrium equation on the tunnel centreline from the tunnel crown up to the ground surface. These two analytical solutions have been validated against five previously published centrifuge tests.

KEYWORDS: clays; deformation; design; plasticity; theoretical analysis; tunnels

On introduit ici une nouvelle méthode analytique pour le calcul de déplacements dus au creusement d'un tunnel. Cette approche est conçue dans le cadre du théorème de la limite de plasticité, permettant toutefois l'écrouissage du sol. Les déplacements du sol provoqués par le creusement d'un tunnel sont idéalisés par un simple mécanisme de déplacement de cisaillement réparti dans le plan de la section transversale du tunnel. La pression de soutènement du tunnel correspondant à une certaine perte de volume est calculée à partir de bilans d'énergie du travail dissipé dans le cisaillement réparti, de la perte d'énergie potentielle de terre s'écoulant dans le tunnel et du travail fourni par ce sol contre la pression de soutènement du tunnel. Les calculs sont effectués par étape de petite perte de volume accompagnant une faible réduction de la pression de soutènement, après chacune desquelles la géométrie du tunnel est réactualisée. De cette manière, chaque pression réduite de soutènement du tunnel est liée à un champ complet de déplacements du sol. Une solution de forme fermée est également fournie pour prédire le tassement maximum du sol en surface généré pour le cas particulier de creusement de tunnel profond. Cette solution de forme fermée est obtenue en intégrant l'équation d'équilibre vertical sur la ligne centrale du tunnel de la voûte du tunnel à la surface au sol. La comparaison avec cinq essais au centrifuge précédemment publiés a permis de valider ces deux solutions analytiques.

INTRODUCTION

The need for construction of tunnels in urban areas requires control of ground movements, because excessive deformations can damage adjacent structures. Engineers usually rely either on empirical observations or on complex finite element analysis to predict displacements around tunnels. Relatively few analytical solutions are available. Sagaseta (1987) presented a closed-form solution for obtaining the strain field around a tunnel excavation within an isotropic, homogeneous, and incompressible material. The soil is modelled as a linear-elastic material. This solution is based on fluid mechanics concepts. First the effect of the soil surface is neglected and the strains due to an assumed sink in an infinite medium are calculated. Then the stresses at the top plane representing the soil surface are eliminated by imposing either a virtual source or sink within the infinite medium and located in a symmetrical position above the plane. These free surface corrections lead to additional components of strain. Verruijt & Booker (1996) extended Sagaseta's solution for compressible materials and include the effects of ovalisation of tunnel openings. However, it is found that Verruijt & Booker's solution gives a wider surface settlement profile and larger horizontal movements than observed in practice. Loganathan & Poulos (1998) modified Verruijt & Booker's solution to give narrower settlement troughs and to account empirically for construction effects.

In the analytical solutions mentioned above, the soil is modelled as a linear-elastic material. However, the stress–strain behaviour of soil is non-linear even at very small strains (Jardine *et al.*, 1984; Burland 1989; Houlsby & Wroth, 1991). Finite element analyses of modelling tunnel construction of the Jubilee Line Extension (JLE) beneath St James's Park conducted by Addenbrooke *et al.* (1997) showed that modelling soil as a linear-elastic material leads to inadequate displacement prediction.

Osman *et al.* (2006) developed a kinematic plastic solution for ground movements around a shallow, unlined, tunnel embedded within an undrained clay layer. In this solution, the pattern of deformation around the tunnel is idealised by a simple plastic deformation mechanism (Fig. 1). Within the boundaries of the deformation mechanism, the soil deforms compatibly, following a Gaussian distribution. Outside this mechanism the soil is assumed to be rigid. This mechanism does not incorporate slip surfaces. Osman *et al.* (2006) demonstrated that the upper bound theorem applied to distributed shearing mechanism offered a reasonable assessment for collapse, and also matches the displacement field observed in centrifuge tests of tunnel failure in clay (Mair, 1979). It was also demonstrated that the shape of the surface settlement profile remained the same as the magnitude of settlement increased towards failure. In this paper it will be demonstrated that an upper bound style of calculation is also capable of predicting ground displacements at any stage prior to failure, representing the soil as a strain-hardening plastic material.

Manuscript received 18 April 2006; revised manuscript accepted 21 September 2006.
Discussion on this paper closes on 1 May 2007, for further details see p. ii.
* School of Engineering, Durham University, UK.
† Department of Engineering, University of Cambridge, UK.

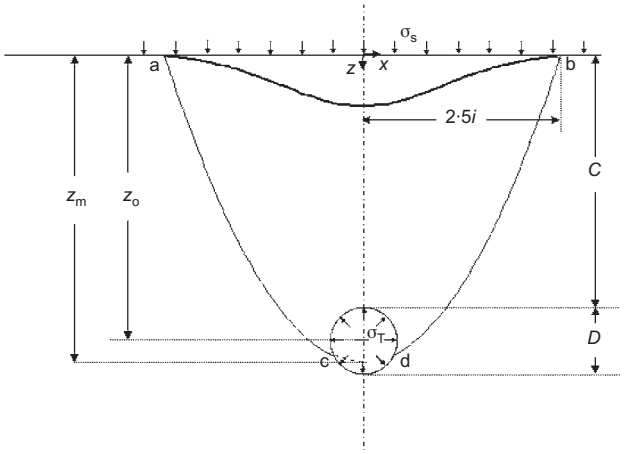

Fig. 1. Plastic deformation mechanism for tunnels in clay

DEFORMATION MECHANSIM

The vertical displacements of the ground surface above a tunnel can be represented by a Gaussian curve (Peck, 1969; Mair & Taylor, 1997), and this is consistent with a considerable amount of field data. The vertical displacements in the deformation mechanism (Fig. 1) proposed by Osman *et al.* (2006) are taken to follow a Gaussian distribution on each successive horizontal plane at depth z below the surface. The distance to the point of inflexion i_z is then expressed by

$$i_z = K_z z_o \tag{1}$$

where

$$K_z = 0{\cdot}5\left(1 - \frac{z}{z_m}\right)^{\alpha} \tag{2}$$

where z_o is the depth of the tunnel centre below the ground surface, z_m is the depth below the ground surface of the point of intersection of the extension of the boundary ac (and bd) with the vertical centreline of the tunnel, and exponent α is taken to be a constant.

At the ground surface, $K_{z=0} = 0{\cdot}5$, which is consistent with a large number of case histories (Rankin, 1988; Mair & Taylor, 1997).

The vertical displacement v is therefore given by

$$v = \frac{As_m}{2K_z}\left\{\exp\left[-\frac{1}{2}\left(\frac{x}{i_z}\right)^2\right] - \exp\left(-\frac{B^2}{2}\right)\right\} \tag{3}$$

and the horizontal displacement u is given by

$$u = -\frac{\alpha A s_m x}{2K_z(z_m - z)}\left\{\exp\left[-\frac{1}{2}\left(\frac{x}{i_z}\right)^2\right] - \exp\left(-\frac{B^2}{2}\right)\right\} \tag{4}$$

where A and B are constants.

Equations (3) and (4) satisfy the incompressibility condition

$$\frac{\partial u}{\partial x} + \frac{\partial v}{\partial z} = 0 \tag{5}$$

The total half-width of the surface settlement trough is assumed to be $2{\cdot}5i$ (Mair *et al.*, 1993), and the soil outside the mechanism is assumed to be stationary, with the maximum surface settlement s_m occurring at the tunnel centreline ($z = 0$, $x = 0$). By satisfying these boundary conditions, it can be shown that B takes the value 2·5 and A takes the value 1·046.

HYPOTHESIS

In order to avoid the complex 3D moving-boundary problem of real tunnel excavation at a face, the mechanism to be developed here will be based on plane-strain cavity contraction (Fig. 1). Here, the cylindrical cavity representing the future tunnel is 'wished into place' and kept open initially by an interior support pressure σ_T, which is taken as the pre-existing vertical stress in the ground at the elevation of the tunnel axis. Tunnel excavation is then simulated in plane strain by steadily reducing σ_T and by monitoring the reduction in the area of the cavity. The mechanical efficiency of a tunnelling operation is usually measured in term of volume loss V_L, expressed as the volume of extra material excavated divided by the intended volume of the tunnel, and expressed as a percentage. When tunnelling in undrained clay, this volume loss is available as the source of a settlement trough expressed at the ground surface.

The total displacements around circular tunnels in working conditions are idealised by the deformation mechanism shown in Fig. 1. The tunnel support pressure σ_T corresponding to a certain volume loss can be calculated from the total energy balances of the work dissipated in distributed shear, the potential energy loss of soil flowing into the tunnel, and the work done by the soil against the tunnel support pressure and on the soil by any surface surcharge pressure σ_S,

$$\int_{-1{\cdot}25z_o}^{1{\cdot}25z_o} (\sigma_S - \sigma_T) v_{z=0} \mathrm{d}x + \int_{Area} \gamma v \mathrm{d}Area = \int_{Area} t\varepsilon_s \mathrm{d}Area \tag{6}$$

where t is the shear strength mobilised under working conditions, and equal to half the difference between the major and the minor principal stresses; σ_T is the tunnel support pressure; σ_S is the surcharge pressure at the ground surface; *Area* is the area of the displacement mechanism shown in Fig. 1; and ε_s is the engineering shear strain, defined as the difference between major and minor principal strain (the expression for ε_s is given in Appendix 2).

The energy calculations given by equation (6) depend on the geometry of the deformation mechanism of Fig. 1. An iteration on the exponent α, which governs the width of the deformation mechanism (equation (2)), and on the depth z_m needs to be carried out in the spirit of upper bound plasticity analysis, to find the critical values that maximise the required tunnel support for any given volume loss. During tunnel construction, of course, the unsupported heading can get the additional benefit of 3D arching, which will reduce the required tunnel support pressure below the 2D calculation that is currently being developed.

CALCULATION METHOD

Change of tunnel geometry during construction

Analytically, a reduction of tunnel support pressure creates a reduction in tunnel diameter. In real tunnel construction the extra material is removed at the face. In the physical model tests that can be used to calibrate an emerging analysis, it is more convenient simply to monitor the reducing tunnel diameter. In this latter case, however, the stability of the tunnel is enhanced by the increasing cover/depth ratio, and it may be necessary to allow for this change of geometry in the analysis of large volume losses occurring in the physical model.

It is proposed to validate the new 2D analysis using centrifuge models constructed at 1*g*, and supported by compressed air at enhanced gravity prior to the compressed air pressure being reduced until the tunnel collapses. In this case, a large volume loss is recorded as the tunnel diameter reduces, and a first-order correction for this finite deforma-

tion must be incorporated. The equivalent diameter D_f of the tunnel (Fig. 2) after each increment of relative volume loss V_L is assumed to be given by

$$D_f = D\sqrt{(1 - V_L)} \tag{7}$$

where D is the initial diameter of the tunnel.

The relative volume loss V_L is calculated in practice (Mair *et al.*, 1993) by

$$V_L = \frac{\sqrt{2\pi}is_m}{\pi D^2/4} \tag{8}$$

Centrifuge models conducted by Mair (1979) showed significant inward displacements occurring at the tunnel crown and shoulders, whereas a much smaller movement was observed at the tunnel invert. The proposed plastic mechanism shown in Fig. 1 implies zero displacement at the tunnel invert. Therefore it is assumed that the location of the invert is fixed and that the cross-section remains circular, as shown in Fig. 2. The centrifuge tests could continue even beyond a volume loss of 50%, because the reduction in tunnel diameter also increases the stability of the remaining cavity, as will be explained below. Tunnel excavations that create more than 5% volume loss might be regarded as problematic in practice.

Calculation steps

The calculations are carried out in steps of small volume loss, after each of which the tunnel geometry is updated. The equivalent diameter of the tunnel at the beginning of the step is calculated from the volume loss at the end of the previous step using equation (7). The incremental volume loss in the next step is then imposed and the corresponding ground displacements are then calculated. Displacements are differentiated to obtain strains, and the new value of maximum shear strain is calculated at every point within the deformation mechanism. Mobilised shear stress can then be read off a representative shear stress–strain curve. The required tunnel support pressure is then calculated from the work equation (equation (6)) by balancing the internal dissipation in distributed shear and the work done against the tunnel supporting pressure, against the work done by the surface surcharge and gravity. The calculations are repeated for different mechanism parameters of α and z_m to find the maximum required value of tunnel support pressure. This is taken as the best available estimate, in the spirit of upper bound plasticity calculations.

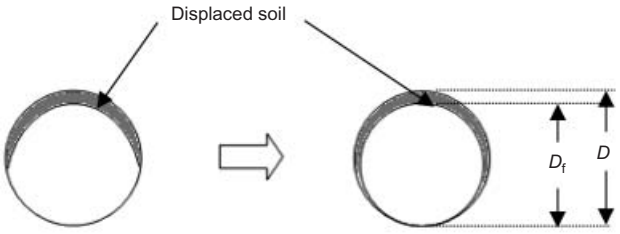

Fig. 2. Idealisation of tunnel geometry

VALIDATION

The proposed calculation method is validated by comparing its predictions with the results of five centrifuge tests conducted by Mair (1979) using the 8 m diameter Cambridge Geotechnical Centrifuge. Table 1 summarises the centrifuge tests used in the back-analysis, and Fig. 3 shows the soil conditions in these tests. Model tunnels were constructed in soft clay and tested at accelerations of 75g and 125g to establish the internal consistency of the method. The clay in test 2DH has constant undrained shear strength with depth. In the other tests, the clay was brought into equilibrium in the centrifuge in an overconsolidated state with a high groundwater table so that the undrained strength increased with depth. In each test, compressed air equal to the total overburden pressure at tunnel axis level was used to support the tunnel as the centrifuge acceleration was applied, and was then reduced incrementally to simulate tunnel excavation. Tests 2DT and 2DU were designed to model tests 2DP and 2DV respectively, at a different scale.

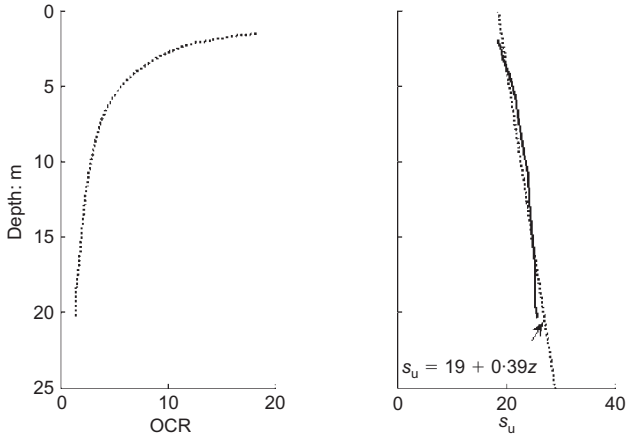

Fig. 3. Conditions for tunnel model in Series II (Mair, 1979)

Table 1. Centrifuge tests, conducted by Mair (1979), used in the validation

Test no.	Cover to diameter ratio, C/D	Laboratory consolidation pressure: kPa	Centrifuge acceleration: g		Tunnel diameter, D: mm	Undrained shear strength, s_u
			Acceleration at base of model	Average acceleration in model		
2DH	1·8	171	75	71	60	Constant undrained shear strength $s_u = 26$ kPa
2DP	1·67	171	75	71	60	Varies with depth (see Fig. 3)
2DV	3·11	171	75	71	60	Varies with depth (see Fig. 3)
2DT	1·67	171	125	119	36	Varies with depth (see Fig. 3)
2DU	3·11	171	125	119	36	Varies with depth (see Fig. 3)

Stress–strain response

Figure 4 shows the direction of principal strain for different soil elements around a tunnel in undrained clay observed in a 1*g* experiment conducted by Seneviratne (1979). In locations above the tunnel crown, and along its vertical centreline, the direction of principal strain is horizontal, which resembles the conditions in plane-strain extension tests. The principal strains in the elements at the tunnel sides are vertical, which resembles the conditions in plane-strain compression tests. Fig. 5(a) shows the results of one-dimensionally consolidated undrained plane-strain compression and extension tests for samples of spestone kaolin clay, which was very similar to the speswhite kaolin clay used in the centrifuge tests listed in Table 1. The plane-strain soil tests were conducted by Sketchley (1973). The stress–strain curves are plotted as shear stress t normalised by the mean effective consolidation stress s'_c. Fig. 5(a) shows behaviour that is typical for normally and lightly overconsolidated materials. In compression, the shear stress reaches a peak value at a shear strain of 6–8%. In contrast, the peak shear stress in extension was mobilised at a much larger shear strain (18–22%). These stress–strain responses, plotted as normalised shear strength (t/s_u) against shear strain ε_s, are shown in Fig. 5(b) together with representative stress–strain curves used in the back-analysis. These curves are taken to represent the possible bounds of the stress–strain response in the experiments. Simple power curves are used to model stress–strain response (Gunn, 1993):

$$\frac{t}{s_u} = \left(\frac{\varepsilon_s}{\varepsilon_{s,f}}\right)^{\beta} \tag{9}$$

From the stress–strain data shown in Fig. 5(b), the exponent β is taken to be 0·15 for compression and 0·5 for extension, and the shear strain at the maximum shear strength, $\varepsilon_{s,f}$, is taken to be 8% and 18% for compression and extension respectively. Large-strain behaviour is assumed to be perfectly plastic.

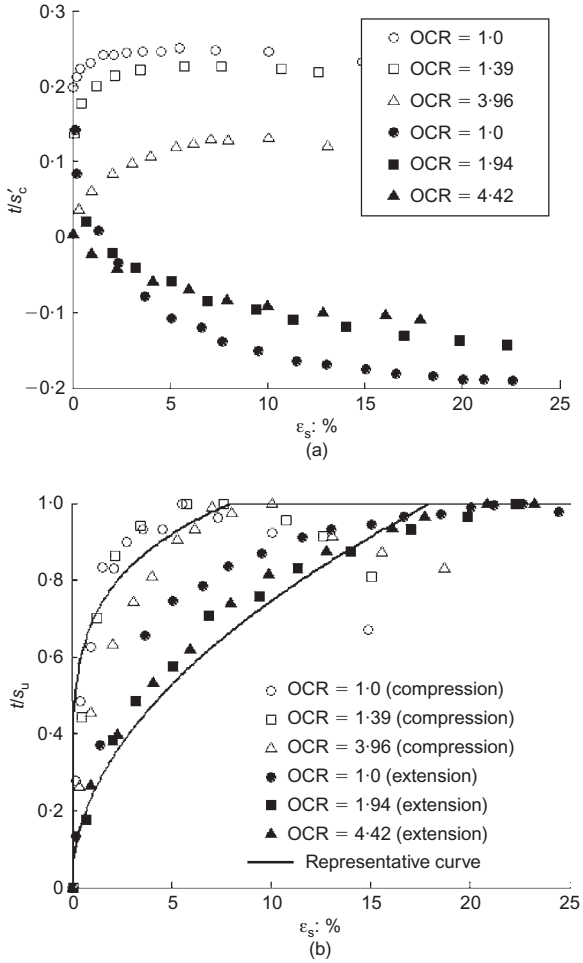

Fig. 5. Stress–strain curves from undrained plane-strain tests in compression and extension on one-dimensionally consolidated spestone clay (after Sketchley, 1973): (a) shear stress normalised by mean effective consolidation stress; (b) shear stress normalised by undrained shear strength

Surface settlement profile

Figure 6 shows observed and calculated maximum mid-surface settlement s_m normalised by tunnel diameter, plotted against reducing tunnel support pressure σ_T. The solid lines show prediction bounds based on the compression and extension stress–strain data of Fig. 5(b). The dotted line presents the settlements calculated from the average of the plane extension and compression data. An example demonstrating the calculation is shown in Appendix 1.

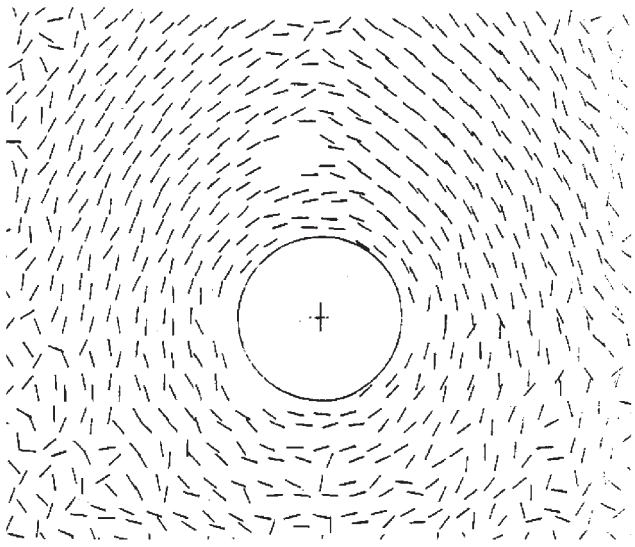

Fig. 4 Direction of major principal strains observed in 1*g* test on a tunnel model in undrained clay (Seneviratne, 1979)

Figure 6 shows that these calculations, assuming isotropic soil behaviour and using either plane-strain extension or plane-strain compression data, do indeed offer bounds for the predicted surface settlements of shallow tunnels (tests 2DH, 2DP and 2DT). The average settlement curve plotted by taking the average values of the calculated settlement based on extension and compression data conforms reasonably to the measured data. The discrepancy at small settlements might be due to inaccuracy in measuring soil stiffness at small strain level in Sketchley's plane-strain tests. For deeper tunnels, 2DV and 2DU, the method overpredicts the settlement by a factor of roughly 2. Alternatively, the calculation of the tunnel support pressure necessary to restrict settlement to a particular value has been underestimated by about 20% for the deep tunnels. These deep tunnel tests were continued until the original cavity was filled with clay. The tendency for stabilisation due to reducing cavity diameter in the later stages of tests 2DV and 2DU is captured, albeit approximately, by the predictions.

Shear strain contours

Figure 7(a) shows the shear strain contours for test 2DP at a volume loss of 42%, and Fig. 8(a) shows the shear strain

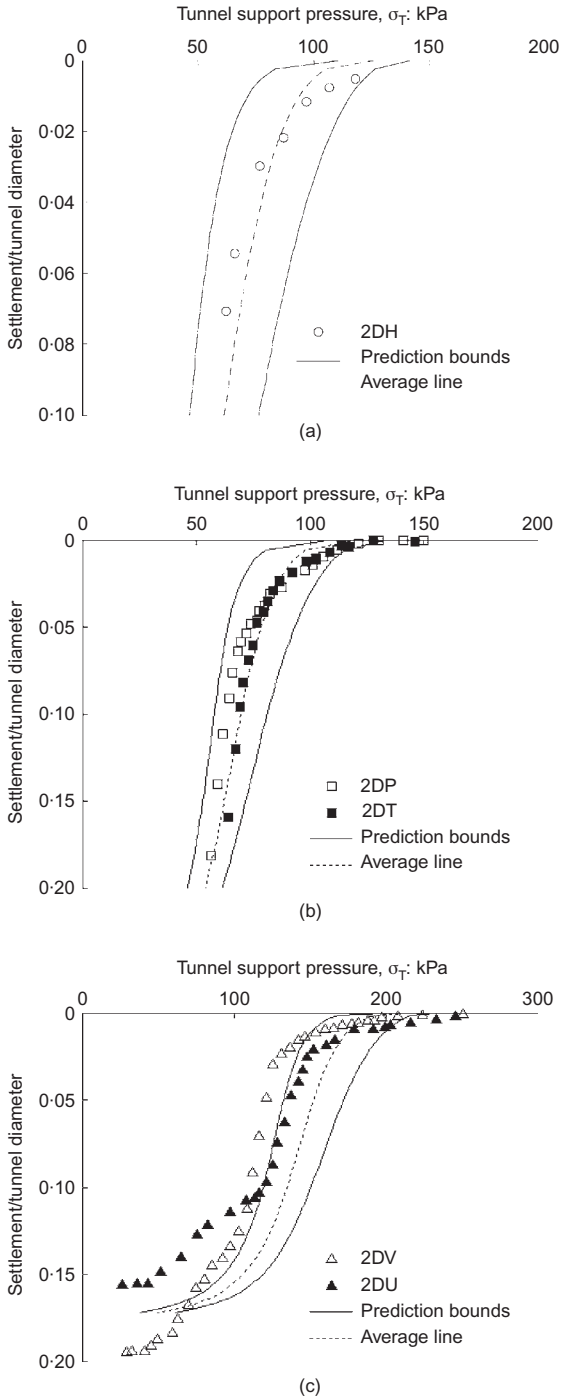

Fig. 6. Mid-surface settlements: (a) $C/D = 1{\cdot}8$; (b) $C/D = 1{\cdot}67$; (c) $C/D = 3{\cdot}11$

contours for test 2DV at a volume loss of 54%, both of which would be regarded as catastrophic in practice. The observed pattern is characterised by regions of intense shearing spreading upwards and outwards from the tunnel shoulders. The shear strain contours calculated from the deformation mechanism using the expression given in Appendix 2, and the average of the predictions obtained from stress–strain responses in extension and compression, are shown for corresponding volume losses in Figs 7(b) and 8(b). The pattern and the magnitudes of the calculated shear strain contours are generally consistent with the observations, although the centrifuge tests indicate that the region above the tunnel crown tends to punch downwards as a block.

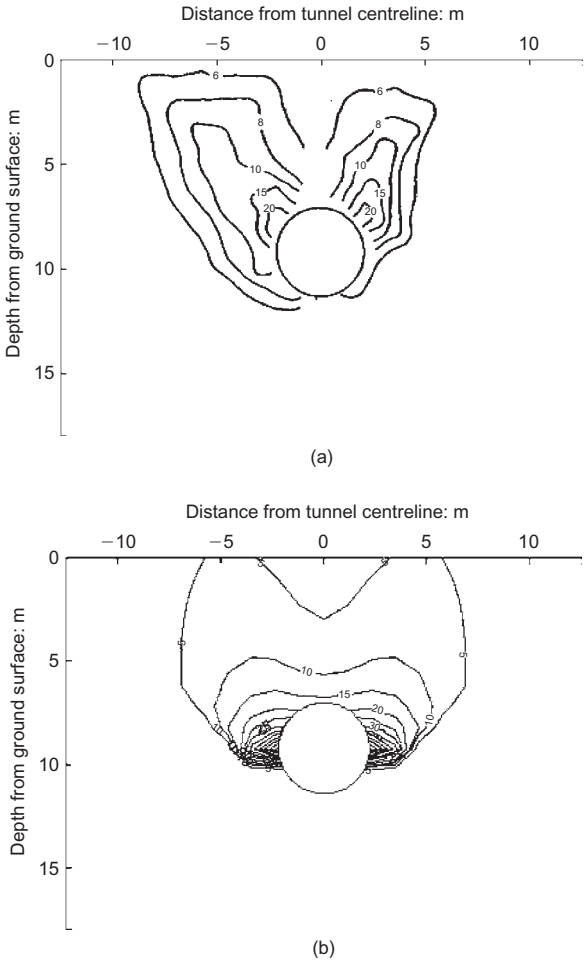

Fig. 7. Comparison between observed and predicted shear strain contours for test 2DP ($V_L = 42\%$): (a) observed shear strain contours; (b) calculated shear strain contours

APPROXIMATE SOLUTION BASED ON RADIAL SYMMETRY

The solution described above is based on a kinematically admissible deformation mechanism that is consistent with observations in centrifuge tests and field data. In this section an approximate closed-form solution is developed based on an assumption of radial symmetry and satisfying the equilibrium condition on the tunnel centreline.

Assuming radial symmetry, the equilibrium equation for a soil element at the tunnel centreline (Fig. 9) can be expressed in polar coordinates as

$$\frac{\mathrm{d}\sigma_r}{\mathrm{d}r} + \frac{\sigma_r - \sigma_\theta}{r} = -\gamma \tag{10}$$

where r is the radial distance from the tunnel centreline, σ_r and σ_θ are the stresses in the radial and circumferential directions respectively, and γ is the unit weight of soil.

The principal strains are in the radial and circumferential directions, and could be assumed to be given by $-v/r$ and v/r, so the shear strain is given by $2v/r$. This kinematical assumption will not be consistent with field observations of shallow tunnels. However, the purpose is to obtain a simple closed-form solution. The relation between the shear strain at ground surface and the shear strain at any point along the vertical plane of symmetry will, if the radial symmetry is invoked, be given by

$$\varepsilon_s = \varepsilon_{s,R_s}\left(\frac{R_s}{r}\right)^2 \tag{11}$$

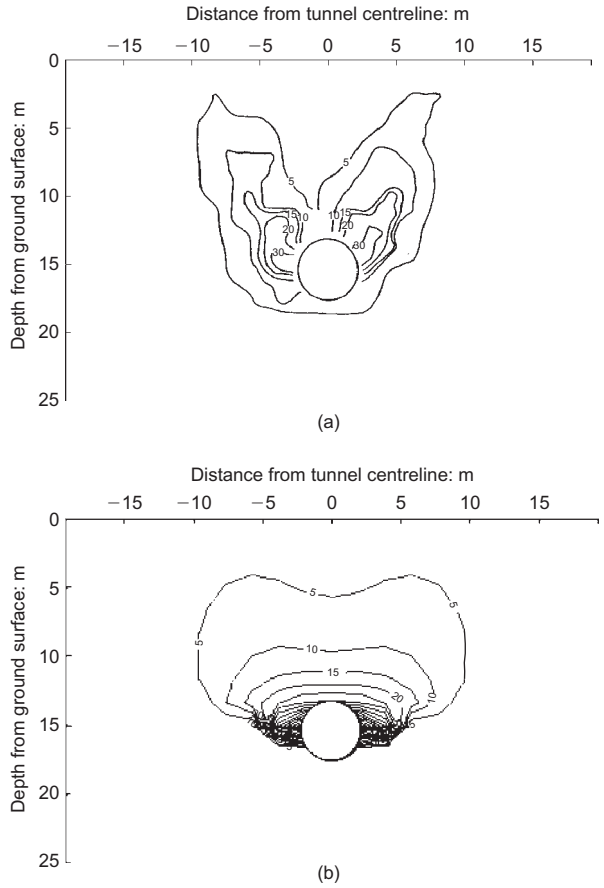

Fig. 8. Comparison between observed and predicted shear strain contours for test 2DV ($V_L = 54\%$): (a) observed shear strain contours; (b) calculated shear strain contours

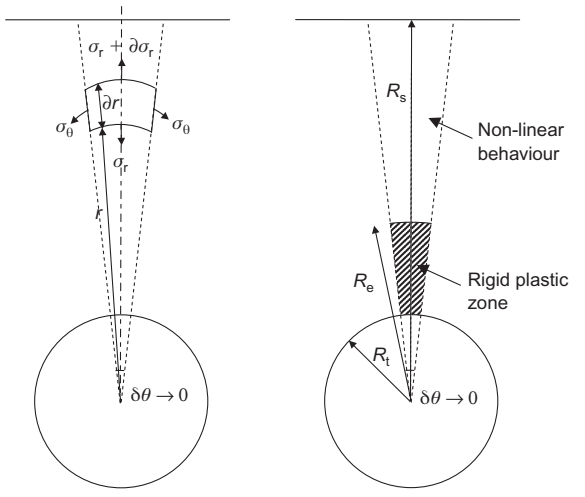

Fig. 9. Simplified equilibrium assumption for tunnels

where R_s is the radial distance from the centre of the tunnel to the ground surface, and ε_{s,R_s} is the engineering shear strain at the ground surface at the centreline of the tunnel (see Fig. 9).

The shear stress t is equal to the half the difference between the major principal stress (the circumferential stress σ_θ) and the minor stress (the radial stress σ_r). If the shear strain is less than the failure shear strain $\varepsilon_{s,f}$ at peak strength, the soil will be assumed to behave as a non-linear material described by equation (9). By combining equations (9) and (11),

$$\frac{d\sigma_r}{dr} - \frac{2s_u}{r}\left(\frac{2s_m R_s}{\varepsilon_{s,f} r^2}\right)^{\beta} = -\gamma \tag{12}$$

Integrating equation (12) gives

$$\sigma_S - \sigma_e = -\gamma(R_s - R_e) - \frac{s_u}{\beta}\left(\frac{2s_m R_s}{\varepsilon_{s,f}}\right)^{\beta}\left(\frac{1}{R_s^{2\beta}} - \frac{1}{R_e^{2\beta}}\right) \tag{13}$$

where σ_e is the radial stress at the upper edge of the fully plastic zone, and R_e is the radial distance from the tunnel centreline to the point whose strain is equal to the failure strain and is given by

$$R_e = \sqrt{\frac{2s_m}{\varepsilon_{s,f}} R_s} \tag{14}$$

In the interior region in which the soil behaves as a fully plastic material, with $t = s_u$, the equilibrium equation can be written as

$$\frac{d\sigma_r}{dr} - \frac{2s_u}{r} = -\gamma \tag{15}$$

and integration gives

$$\sigma_e - \sigma_T = -\gamma(R_e - R_T) - s_u \ln\left(\frac{R_e^2}{R_T^2}\right) \tag{16}$$

By combining equations (13) and (16)

$$\sigma_S - \sigma_T = -\gamma(R_s - R_T) - \frac{s_u}{\beta}\left(\frac{2s_m R_s}{\varepsilon_{s,f}}\right)^{\beta} \times \left(\frac{1}{R_s^{2\beta}} - \frac{1}{R_e^{2\beta}}\right) - s_u \ln\left(\frac{R_e^2}{R_T^2}\right) \tag{17}$$

Figure 10 shows the settlement profile predicted by equation (17). The extension data are used here, because the major principal strain direction along the centreline is always horizontal, as shown in Fig. (4). The calculations are carried out in steps of 1% volume loss, and the equivalent tunnel diameter is calculated from equation (7). The soil is assumed to be homogeneous, and the average undrained shear strength above the tunnel is used in the calculations. It appears that this simple closed-form solution underestimates the required 2D tunnel support pressure by about 20% for shallow tunnels but fits reasonably well with the data of deeper tunnels ($C/D = 3{\cdot}11$) in the earlier stages of simulated excavation before overestimating required support by about 10% at a settlement/diameter ratio of about 10%. The discrepancy is due mainly to the assumption of a radially symmetrical displacement field. This solution is based on homogeneous soil with constant shear strength.

CONCLUSION

The ground displacements due to tunnelling are idealised by a simple plane-strain displacement mechanism. The soil is assumed to deform compatibly and continuously following a Gaussian distributed curve of vertical displacements. The calculations are carried out in steps of small volume loss, after each of which the tunnel geometry can be updated. A simplified expression to account for change of tunnel geometry is assumed. The required tunnel support pressure corresponding to a certain volume loss is calculated from a work equation by balancing the work done by gravity, and any surface surcharge, against the work done on tunnel support pressure, and the energy dissipated in distributed shearing. A conservative approach is adopted by seeking the

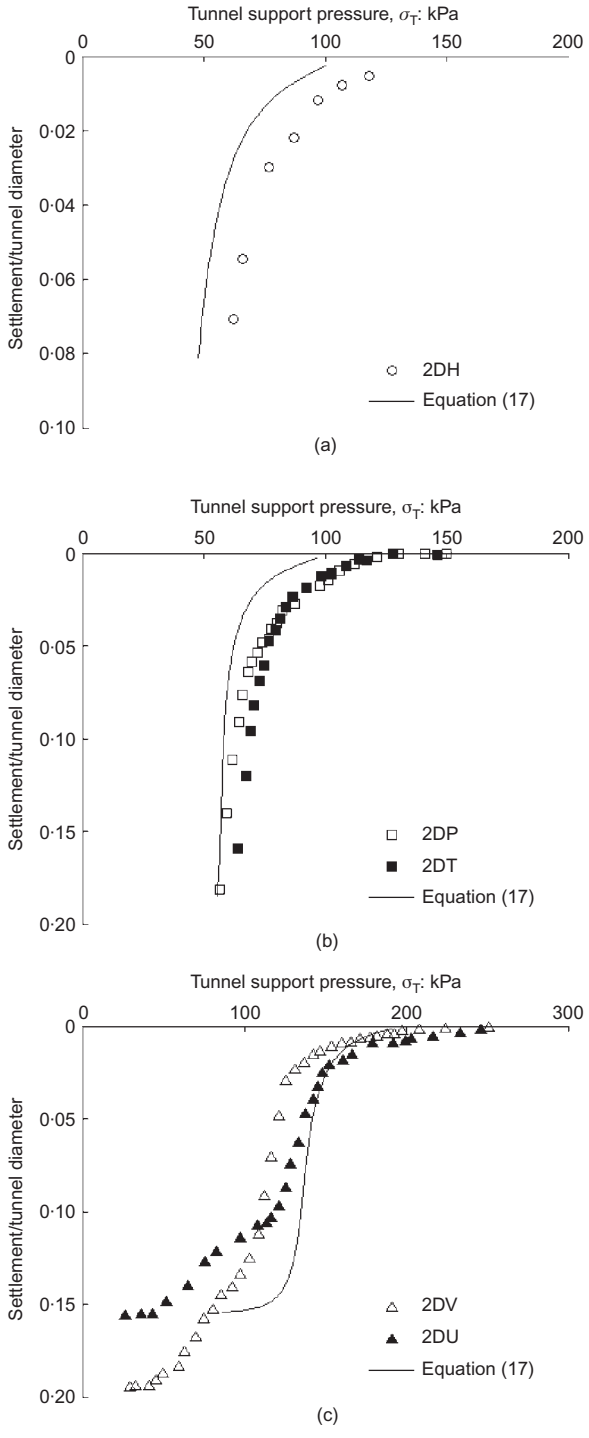

Fig. 10. Mid-surface settlement predicted using equation (17): (a) $C/D = 1{\cdot}8$; (b) $C/D = 1{\cdot}67$; (c) $C/D = 3{\cdot}11$

maximum required tunnel support pressure, which is obtained by iterating for a variety of deformation mechanisms in the spirit of upper bound limit analyses. Here, however, the calculation is of the tunnel support pressure required to limit ground settlements to given magnitudes.

The calculation method is validated by five centrifuge tests on plane-strain unlined tunnels in kaolin clay. The behaviour of the clay is simplified by fitting the stress–strain data of biaxial extension and compression tests with simple power curves. The observed data appear to be confined within the predicted range of settlements. The average settlement curves plotted by taking the average values of the calculated settlement based on extension and compression data conform closely to the measured data. However, this appears to be conservative for deep tunnels, overpredicting the tunnel support pressure by about 20%.

The authors also developed a simple closed-form solution for the prediction of maximum surface ground settlement. This solution is obtained by integrating the equilibrium equations along the tunnel centreline from the tunnel circumference up to the ground surface and by invoking radial symmetry. A simple power curve was used to model the stress–strain relations. These analytical solutions for maximum surface settlements have also been validated against the centrifuge test data, and gave close correspondence for deep tunnels but underpredicted tunnel support pressure by about 20% for shallow tunnels ($C/D < 3$).

ACKNOWLEDGEMENTS

The authors acknowledge the support of the Engineering and Physical Sciences Research Council (EPSRC): Platform Grant GR/T 18660/01.

APPENDIX 1. CALCULATIONS ILLUSTRATION

In test 2DH (Mair, 1979), the bulk unit weight of the soil is 15·9 kN/m^3, the cover to depth ratio C/D is 1·8, the tunnel diameter is 60 mm, and the average centrifuge acceleration is 71g. The prototype tunnel diameter is therefore 4·26 m and the prototype depth to the tunnel axis z_o is 9·78 m. The calculations are carried out in small increments of volume loss. The increment size is chosen to be 1%. The potential energy loss and the work dissipated in distributed shear need to be calculated. Let us first assume that the mechanism parameters are $\alpha = 0{\cdot}35$ and $(z_m - z_o)/(D/2) = 0{\cdot}45$. From equation (2), the width parameter i at the ground surface is equal to $0{\cdot}5z_o$. The maximum mid-surface settlement s_m is calculated from the relative volume loss using equation (8):

$$s_m = \frac{V_L \pi D^2}{4\sqrt{2\pi} i} = \frac{1}{100} \times \frac{\pi \times 4{\cdot}26^2}{4\sqrt{2\pi}(0{\cdot}5 \times 9{\cdot}78)} = 0{\cdot}0116 \text{ m}$$

i is taken to be equal to $0{\cdot}5z_o$ (equation (1)): thus the maximum mid-surface settlement s_m is found to be 0·0116 m.

In a soil element located at a depth z of 4 m below the ground surface and a horizontal distance x of 1 m from the centreline, the vertical displacement v found from equation (3) is 0·0127 m, which gives a potential energy loss per unit volume of 0·2018 kN m. The shear strain ε_s (calculated from the expression given in Appendix 2) at the end of the step is 0·0015. At a depth of 4 m the undrained shear strength, from Fig. 3, is 20·6 kPa.

The pre-peak behaviour is modelled by a simple power curve expressed by equation (9). The internal work per unit volume dissipated in the distributed shear zone using the plane extension data curve ($\beta = 0{\cdot}5$, $\varepsilon_{s,f} = 0{\cdot}18$) is therefore

$$\frac{s_u}{\beta + 1}\left(\frac{\varepsilon_s}{\varepsilon_{s,f}}\right)^{\beta+1} = \frac{20{\cdot}56}{1 + 0{\cdot}5}\left(\frac{0{\cdot}0015}{0{\cdot}18}\right)^{0{\cdot}5+1} = 0{\cdot}002 \text{ kNm/m}^3$$

The integration of the work equation (equation (8)) needs to be carried out for the whole volume of the deformation mechanism of Fig. 1. The gives $\sigma_T = 92$ kPa. The values of α and z_m are iterated until a maximum value of tunnel support is achieved, which is found to be 141·5 kPa.

At the end of this step of calculation the equivalent tunnel diameter from equation (9) will be 4·24 m. The energy calculation is repeated in the further steps as requested, with $V_L = 2\%$ and $D = 4{\cdot}24$ m, etc.

APPENDIX 2. ENGINEERING SHEAR STRAIN

The engineering shear strain ε_s is given by

$$\varepsilon_s = \sqrt{(\varepsilon_x - \varepsilon_z)^2 + \gamma_{xz}^2} = \sqrt{\left(\frac{\partial u}{\partial x} - \frac{\partial v}{\partial z}\right)^2 + \left(\frac{\partial u}{\partial z} + \frac{\partial v}{\partial x}\right)^2} \qquad (18)$$

Substituting equations (3) and (4) into equation (18) gives

$$\varepsilon_s = \frac{A s_m (z_m)^{\alpha}}{(z_m - z)^{\alpha+1}} \left(\left[2\alpha \left(\left\{ 1 - 4 \left[\frac{x(z_m)^{\alpha}}{(z_m - z)^{\alpha} z_o} \right]^2 \right\} \exp\left\{ -2 \left[\frac{x(z_m)^{\alpha}}{(z_m - z)^{\alpha} z_o} \right]^2 \right\} - \exp\left(-\frac{B^2}{2} \right) \right) \right]^2 + \left\{ \frac{x}{(z_m - z)} \left[\alpha(1+\alpha) \left(\left\{ 1 - \frac{4\alpha}{1+\alpha} \left[\frac{x(z_m)^{\alpha}}{(z_m - z)^{\alpha} z_o} \right]^2 \right\} \exp\left\{ -2 \left[\frac{x(z_m)^{\alpha}}{(z_m - z)^{\alpha} z_o} \right]^2 \right\} - \exp\left(-\frac{B^2}{2} \right) \right) + \frac{4(z_m)^{2\alpha}(z_m - z)^{2(1-\alpha)}}{(z_o)^2} \exp\left\{ -2 \left[\frac{x(z_m)^{\alpha}}{(z_m - z)^{\alpha} z_o} \right]^2 \right\} \right] \right\}^2 \right)^{0.5} \quad (19)$$

NOTATION

- A constant in displacement equations
- B constant in displacement equations
- C depth of tunnel cover
- D tunnel diameter
- D_f equivalent tunnel diameter after each increment of volume loss
- i width of surface settlement trough
- i_z width of settlement trough at depth z
- K_z constant relating width of the settlement trough to depth of the tunnel at depth z
- r radial distance from centre of tunnel
- R_e radial distance from centre of tunnel to point whose strain is equal to failure strain
- R_s radial distance from centre of tunnel to ground surface
- R_T radial distance from centre of tunnel to tunnel circumference
- s_m maximum surface settlement
- s_u soil undrained strength
- s_{uo} undrained strength at ground surface
- $s_{u,T}$ soil undrained strength at level of centre of tunnel
- s'_c mean effective consolidation stress
- t shear strength mobilised under working conditions equal to half difference between major and minor principal stresses
- u horizontal displacement
- V_L relative volume loss
- v vertical displacement
- x lateral displacement from vertical centreline of tunnel
- z depth below ground surface
- z_m depth below ground surface of point of intersection of extension of vertical boundaries of deformation mechanism with extension of vertical centreline of tunnel
- z_o depth to centre of tunnel
- α constant controlling vertical curvature of outer boundary of plastic deformation mechanism.
- β power exponent in stress–strain power curve
- γ unit weight of soil
- γ_{xz} shear strain in x–z plane
- ε_s engineering shear strain
- $\varepsilon_{s,f}$ engineering shear strain at maximum shear strength
- ε_{s,R_s} engineering shear strain at ground surface at centreline of tunnel
- ε_x strain in horizontal direction (x-direction)
- ε_z strain in vertical direction (z-direction)
- σ_θ circumferential stress
- σ_e radial stress at upper edge of fully plastic zone
- σ_r radial stress
- σ_S surface surcharge pressure
- σ_T tunnel supporting pressure

REFERENCES

Addenbrooke, T. I., Potts, D. M., & Puzrin, A. M. (1997). The influence of pre-failure soil stiffness on the numerical analysis of tunnel construction. *Géotechnique* **47**, No. 3, 693–712.

Burland, J. B. (1989). 'Small is beautiful': the stiffness of soils at small strains. Ninth Laurits Bjerrum Memorial Lecture. *Can. Geotech. J.* **26**, No. 4, 449–516.

Gunn, M. J. (1993). The prediction of surface settlement profiles due to tunnelling. In *Predictive soil mechanics* (eds G. T. Houlsby and A. N. Schofield), Proceedings of Wroth Memorial Symposium, pp. 304–314. London: Thomas Telford.

Houlsby, G. T & Wroth, C. P. (1991). Variation of shear modulus of a clay with pressure and overconsolidation ratio. *Soils Found.* **31**, No. 3, 138–143.

Jardine, R. J., Symes, M. J. & Burland, J. B. (1984). The measurement of soil stiffness in the triaxial apparatus. *Géotechnique* **34**, No. 3, 323–340.

Loganathan, N. & Poulos, H. G. (1998). Analytical prediction for tunneling-induced ground movements in clays. *ASCE J. Geotech. Geoenviron. Engng* **124**, No. 9, 846–856.

Mair, R. J. (1979). *Centrifugal modelling of tunnel construction in soft clay.* PhD thesis, University of Cambridge.

Mair, R. J. & Taylor, R. N. (1997). Bored tunnelling in urban environment. *Proc. 14th Int. Conf. Soil Mech. Found. Engng, Hamburg* **4**, 2353–2385.

Mair, R. J., Taylor, R. N. & Bracegirdle, A. (1993). Subsurface settlement profiles above tunnels in clays. *Géotechnique* **43**, No. 2, 315–320.

Osman, A. S., Mair, R. J. & Bolton, M. D. (2006). On the kinematics of 2D tunnel collapse in undrained clay. *Géotechnique* **56**, No. 9, 585–595.

Peck, R. B. (1969). Deep excavations and tunnelling in soft ground. *Proc. 7th Int. Conf. Soil Mech., Mexico City* **3**, 225–290.

Rankin, W. J. (1988). Ground movements resulting from urban tunnelling. *Proceedings of the conference on engineering geology of underground movements*, Nottingham, pp. 79–92.

Sagaseta, C. (1987). Analysis of undrained soil deformation due to ground loss. *Géotechnique* **37**, No. 3, 301–320.

Seneviratne, H. N. (1979). *Deformations and pore pressure variations around shallow tunnels in soft clay.* PhD thesis, University of Cambridge.

Sketchley, C. J. (1973). *Behaviour of kaolin in plane-strain*. PhD thesis, University of Cambridge.

Verruijt, A. & Booker, J. R. (1996). Surface settlements due to deformation of a tunnel in an elastic half plane. *Géotechnique* **46**, No. 6, 753–756.